PHYSICAL REVIEW LETTERS

Universality of Single-Particle Spectra of Cuprate Superconductors

Lijun Zhu, Vivek Aji, Arkady Shekhter, and C. M. Varma

Department of Physics and Astronomy, University of California, Riverside, California 92521, USA

All the available data for the dispersion and linewidth of the single-particle spectra above the superconducting gap and the pseudogap in metallic cuprates for any doping have universal features. The linewidth is linear in energy below a scale ω_c and constant above. The cusp in the linewidth at ω_c mandates, due to causality, a waterfall, i.e., a vertical feature in the dispersion. These features are predicted by a recent microscopic theory. We find that all data can be quantitatively fitted by the theory with a coupling constant λ_0 and an upper cutoff at ω_c, which vary by less than 50% among the different cuprates and for varying dopings. The microscopic theory also gives these values to within factors of $O(2)$.

Introduction.—With increased refinement of technique and imaginative use, angle-resolved photoemission spectroscopy (ARPES) on the high temperature superconductors has revealed that novel physical principles determine the single-particle spectra in such compounds [1,2]. Recently, the single-particle spectra over an energy range from the chemical potential to about 1 eV have been deduced for various metallic dopings in different cuprates [3–10]. Also, recently a microscopic theory [11] has been formulated that derives the fluctuations leading to the phenomenological marginal Fermi liquid (MFL) [12] and their coupling to fermions. MFL had previously been tested only for low energies and near optimal doping in Bi2212 [13–15] with adjustable couplings. Here we test crucial new features of the microscopic theory including its universality, its cutoff, and its coupling functions, by comparing with recent ARPES data in 4 different cuprate families and at different dopings.

The most important results of these recent ARPES experiments may be summarized as follows: (i) The spectra for energies ω in the range of interest (above the superconducting gap and the pseudogap energy scales) are universal; they have the same functional form for all cuprates and for all metallic dopings. Moreover, even the parameters in the functional form vary less than by a factor of 2 over the entire range of cuprates for which data are available, irrespective of whether they are underdoped (UD), optimally doped (OP), or overdoped (OD). (ii) The momentum distribution curves (MDC) at constant energy ω is a Lorentzian with width $w_\mathbf{k}(\omega)$. In the energy range of interest $w_\mathbf{k}$ varies linearly with ω up to a cutoff above which it is approximately a constant. This is modified if the bare velocity $\mathbf{v}(\mathbf{k})$ varies within $w_\mathbf{k}$, which happens as the bottom of the band is approached. See Fig. 3 below for representative experimental data. (iii) The peak of the MDC as a function of ω moves with $\mathbf{k}$ defining the renormalized dispersion $\varepsilon(\mathbf{k})$. The observed dispersion $\varepsilon(\mathbf{k})$ follows the band structure $\epsilon_\mathbf{k}$ with a smooth renormalization factor up to $\omega \approx E_1$. Above E_1, the "velocity" $d\varepsilon(\mathbf{k})/dk$ sharply increases up to another cutoff E_2 where

$\varepsilon(\mathbf{k})$ resumes the normal dispersion. The nearly vertical dispersion has been picturesquely termed a "waterfall" [3]. In the energy range, $E_1 \lesssim \omega \lesssim E_2$, there is also an indication of multiple $\varepsilon(\mathbf{k})$ for fixed ω [6,8]. E_1 varies systematically, being largest in the (π, π) direction and smallest in the $(\pi, 0)$ direction [8]. Similarly, the position of the waterfall in $\mathbf{k}$ space varies systematically.

All these features follow quantitatively from the quantum-critical fluctuations derived recently [11]. We find that, given the bare band structure $\epsilon_\mathbf{k}$, all available data can be fitted with the two parameters of this theory, a sharp cutoff ω_c, and a coupling constant λ_0 calculable to factors of $O(2)$.

Single-particle spectral function.—The single-particle spectral function deduced by ARPES is given as

$$A(\mathbf{k}, \omega) = \frac{-\mathrm{Im}\Sigma(\omega, \mathbf{k})/\pi}{[\omega - \mathrm{Re}\Sigma(\omega, \mathbf{k}) - \epsilon_\mathbf{k}]^2 + [\mathrm{Im}\Sigma(\omega, \mathbf{k})]^2},$$
(1)

where $\Sigma(\omega, \mathbf{k})$ is the self-energy function. The band structure $\epsilon_\mathbf{k}$ is in general fitted by the tight-binding dispersion [16].

Microscopic theory.—A microscopic theory for the cuprates [11,17,18] is based on the realization that the central organizing feature in the physics of the metallic phase of the cuprates are quantum-critical fluctuations of loop currents. In this theory the ordering of these loop currents below T_g (PG in inset of Fig. 1) leads to a phase that breaks time-reversal symmetry but preserves translational symmetry. Direct evidence for such an ordered state has been obtained by polarized neutron scattering in $YBa_2Cu_3O_{6+x}$ [19] and by dichroic ARPES experiments in $Bi_2Sr_2CaCu_2O_{8+x}$ [20], for various x in the pseudogap phase. The properties in the entire funnel shaped region (I) in the inset of Fig. 1 are determined by the quantum-critical fluctuations of the loop currents. Therefore universal properties are predicted for ω larger than the superconducting gap or the pseudogap for all x in the metallic phases on either side of x_c.
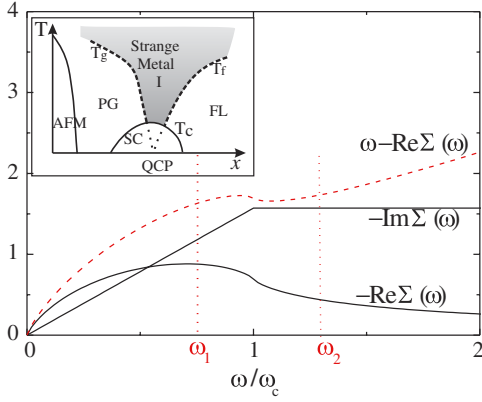
FIG. 1 (color online). The self-energy and $\omega - \mathrm{Re}\Sigma(\omega)$ as functions of ω for $\lambda_0 = 1$. All quantities are dimensionless in units of ω_c. The observable dispersion $\varepsilon(\mathbf{k})$ for a given bare $\epsilon_{\mathbf{k}}$, solved by Eq. (6) is equivalent to the intersection of $\omega - \mathrm{Re}\Sigma(\omega)$ with a horizontal line at $\epsilon_{\mathbf{k}}$. As $\omega - \mathrm{Re}\Sigma(\omega)$ has a wide reentrant region for $\omega_1 \leq \omega \leq \omega_2$, the observed dispersion falls from ω_1 to ω_2 for a very small variation in $\epsilon_{\mathbf{k}}$ producing the waterfall. Inset shows the phase-diagram of the cuprates.

The microscopic theory of the quantum-critical fluctuations [11] gives their absorptive part to be

$$\mathrm{Im}\chi(\mathbf{q}, \nu) = \begin{array}{ll} -\chi_0 \tanh\frac{\nu}{2T}, & |\nu| < \omega_c; \\ 0, & |\nu| > \omega_c. \end{array} \quad (2)$$

ω_c is a cutoff and χ_0 gives the integrated weight of the fluctuations. In the microscopic theory [11], $\omega_c^2 \approx 2EVR^2$, where E is the local repulsion or charging energy parameter, V is the nearest neighbor Cu-O interaction, and R is the dimensionless loop-current order parameter. $\chi_0 \approx R/\omega_c$. For $E \simeq 5$ eV, $V \simeq 1$–2 eV, and $R \simeq 0.1$, which is consistent with the neutron measurements, we expect $\omega_c \approx 0.3$–0.5 eV.

Calculation of the self-energy.—The loop-current fluctuations scatter fermions from $\mathbf{k}$ to $\mathbf{k}'$ with the amplitude $\gamma(\mathbf{k}, \mathbf{k}')$. From the microscopic model, we find [21]

$$\gamma(\mathbf{k}, \mathbf{k}') = \pm i \frac{V}{2}[s_x(k+k')s_y(k-k') - x \leftrightarrow y]S_{xy}(k, k'), \quad (3)$$

where $s_{x,y}(k) \equiv \sin(k_{x,y}a/2)$, $s_{xy}(k) \equiv \sqrt{s_x^2(k) + s_y^2(k)}$, $S_{xy}(k, k') \equiv [s_{xy}^{-1}(k) + s_{xy}^{-1}(k')]$. The leading self-energy contribution is

$$\Sigma(i\omega_n, \mathbf{k}) = T \sum_{\mathbf{q}, i\nu_n} |\gamma(\mathbf{k}, \mathbf{k} + \mathbf{q})|^2$$
$$\times G(i\omega_n + i\nu_n, \mathbf{k} + \mathbf{q})\chi(\mathbf{q}, i\nu_n), \quad (4)$$

where ω_n, ν_n are Matsubara frequencies of the quasiparticle and the fluctuating mode, respectively. Given a $\mathbf{q}$-independent χ and $\gamma(\mathbf{k}, \mathbf{k}')$ of the form of Eq. (3), the self-energy variation with $\mathbf{k}$ on a Fermi surface comes only from the separable s-wave part of $|\gamma(\mathbf{k}, \mathbf{k}')|^2$, which is $\propto (1 - \cos k_x a \cos k_y a)(k \to k')$. This gives $\lambda_k \propto$

$(1 - \cos k_x a \cos k_y a)$, which varies by about a factor of 2 from the (π, π) to the $(\pi, 0)$ directions for the Fermi surface of Bi2212 near optimal doping.

At $T = 0$ the self-energy is easily evaluated to be

$$\mathrm{Im}\Sigma(\omega, \mathbf{k}) = -\lambda(\mathbf{k})\frac{\pi}{2}\begin{cases} |\omega|, & |\omega| < \omega_c \\ \omega_c, & |\omega| > \omega_c \end{cases}$$

$$\mathrm{Re}\Sigma(\omega, \mathbf{k}) = -\frac{\lambda(\mathbf{k})}{2}\left[\omega \ln\frac{\omega_c}{|\omega|}\right.$$
$$\left. + (\omega - \omega_c)\ln\frac{|\omega - \omega_c|}{\omega_c} - (\omega \to -\omega)\right], \quad (5)$$

where $\lambda(\mathbf{k}) = \lambda_0\langle\gamma^2\rangle_{k'}$, $\lambda_0 = N(0)(V^2/4)\chi_0$, and $\langle\gamma^2\rangle_{k'}$ is the average of $|\gamma(\mathbf{k}, \mathbf{k}')|^2$ over $\mathbf{k}'$ on the Fermi surface. For the density of states per one spin species $N(0) \approx 1(eV)^{-1}$ and other parameters used above, we expect $\lambda_0 \approx 1$.

Given such a weakly momentum dependent self-energy, the vertex corrections [22] to the self-energy are only of $O(\lambda\omega_c/W)$, where W is the bare bandwidth of the conduction band. Using the ω_c and λ fitted to the experiments, this ratio is of $O(0.1)$. The remaining processes, repeated scattering (self-consistent Born approximation) produce no singular corrections. At low energies compared to ω_c, Eq. (5) reduces to the MFL form deduced earlier [12], except for the weak momentum dependence.

Given the sharp change of the slope in the imaginary part near ω_c, the real part has a logarithmic divergence in its slope at ω_c before changing from its low energy form $\propto \omega \log|\omega|$ to $1/\omega$ for $\omega \gg \omega_c$. This sharp variation of $\mathrm{Re}\Sigma(\omega)$ near ω_c is responsible for the observed waterfall feature as we now proceed to show.

The waterfall.—The dispersion of the quasiparticles, $\varepsilon(\mathbf{k})$ given by

$$\varepsilon(\mathbf{k}) - \mathrm{Re}\Sigma(\varepsilon(\mathbf{k})) - \epsilon_{\mathbf{k}} = 0. \quad (6)$$

As shown in Fig. 1, $\omega - \mathrm{Re}\Sigma(\omega)$ has a wide reentrant region from $\omega_1 \leq \omega \leq \omega_2$. The solution of Eq. (6) therefore produces a waterfall in the dispersion $\varepsilon(\mathbf{k})$ because it varies over the large energy range ω_1 to ω_2 for a very small variation in $\mathbf{k}$. The multiple solutions obtained in this region are within $\mathrm{Im}\Sigma(\omega)$ for λ of $O(1)$. Above $\omega \simeq \omega_2$, the dispersion becomes just a renormalized band structure. The calculated waterfall is shown in Fig. 2. The spectral intensity maps in Figs. 2(d)–2(f) should be compared with Figs. 1(a)–1(c) of Ref. [8].

Comparison with experiments.—The calculated self-energy at $\lambda_0 = 1$ (suitable to fit the experimental data [8] for $\mathrm{La}_{1.83}\mathrm{Sr}_{0.17}\mathrm{CuO}_4$) is shown in Fig. 1. The experimental MDC width for this compound and the calculated widths for three different cuts are compared with experiment in Fig. 3. In Figs. 4(a)–4(c), we compare the experiments [3] for the dispersion of three Bi2212 samples at different dopings with calculations with $\omega_c = 0.5$, $\lambda_0 \sim 1$. In Fig. 4(d), we compare the measured linewidth for an UD-LSCO sample, an OP-Bi2201 sample and an OP-
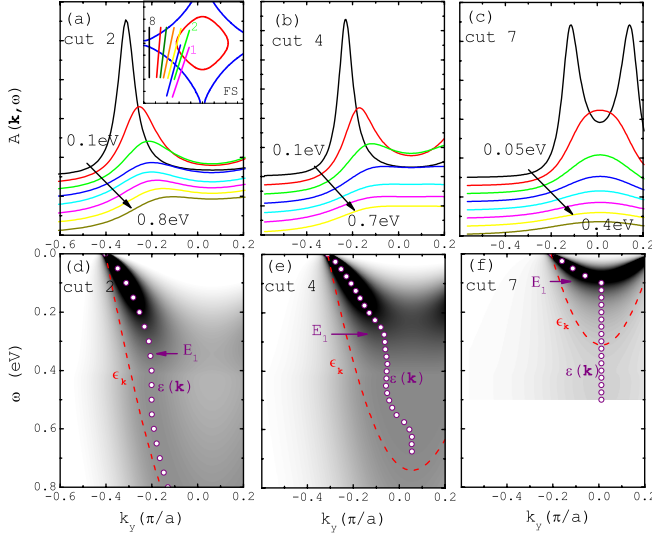
FIG. 2 (color online).   (a),(b),(c) Calculated MDCs for three of the momentum cuts 2, 4, and 7 shown in the inset of (a) for which data are available from Ref. [8]. The MDCs are shown at various energies ω labeled in the figures. (d),(e),(f) Spectral intensity maps for the same cuts correspondingly. From the intensity maps, we can identify the dispersion $\varepsilon(\mathbf{k})$ marked by circles; the bare dispersion $\epsilon_{\mathbf{k}}$ are shown in dashed lines. The inset of (a) shows the Fermi surface and eight momentum cuts done in experiments [8]. It also shows the positions where the waterfall are expected in $\mathbf{k}$ space for radial cuts with the additional contour drawn inside the Fermi surface.

Bi2212 sample with calculations with parameters given in the figure caption.

Universality of the data.—The data and the comparison with experiments in Fig. 3 and 4(a)–4(d) attest to the universality of the single-particle spectra of the cuprates and of the quantitative success of the theory. Now we consider in detail each of the points (i) to (iii) of the experimental data and explain them successively.
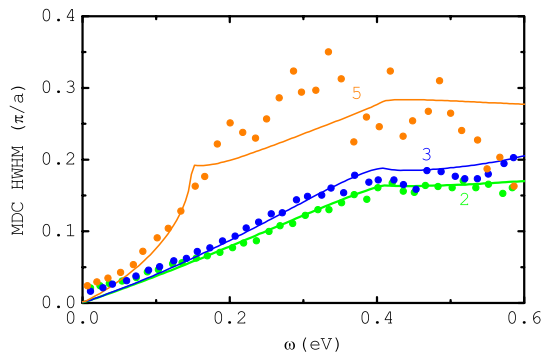

FIG. 3 (color online).   The MDC half-width at half-maximum $w_{\mathbf{k}}(\omega)$ is shown for cuts 2, 3 and 5 of the inset of Fig. 2(a). The experimental data for the same cuts from Fig. 2 of Ref. [8] are also shown. Note that the experiments quoted are done with an energy resolution of 30 meV, which accounts for the deviation from the theory at low energies. Higher resolution data [15] confined to lower energies is consistent with the theory.

(i) The physical properties in any quantum-critical regime are universal, controlled by the scale-invariant critical fluctuations. Specifically, for ω larger than the superconducting gap or the pseudogap the self-energy is of MFL form and is given in terms of only the two parameters ω_c, λ_0 for each compound for all x. Weak dependencies in these parameters from variation in microscopic parameters due to varying x or T may occur, of course. We find, however, that for a given compound, a single value of these parameters is adequate to fit all the available data for different x and for all momentum directions.

It is worth noting that the spectra for energies below the pseudogap energy and $T \leq T_g$ is also scale invariant with a new scale $\propto T_g(x)$ [23,24].

(ii) Suppose at certain energy ω, Eq. (6) is satisfied for $\mathbf{k} = \mathbf{k}_0$. Since the self-energy does not depend significantly on $\mathbf{k}$, we can expand the spectral function in $(\mathbf{k} - \mathbf{k}_0)$. The MDC is then a Lorentzian with width $w_{\mathbf{k}}$ given by $\mathrm{Im}\Sigma(\omega)/\upsilon(\mathbf{k}_0)$ where $\upsilon(\mathbf{k}_0) = \upsilon_y(\mathbf{k}_0) + \upsilon_x(\mathbf{k}_0)(k_x - k_{x0})/(k_y - k_{y0})$, is the bare velocity in the momentum-cut direction. This expansion also requires that within $(\mathbf{k} - \mathbf{k}_0) \approx w_{\mathbf{k}}$, the velocity $\mathbf{v}_{\mathbf{k}}$ is nearly a constant.

As discussed above, $\mathrm{Im}\Sigma(\omega)$ increases linearly in ω for $\omega \lesssim \omega_c$ and is constant beyond. Therefore if $\mathbf{v}_0(\mathbf{k})$ varies slowly with $\mathbf{k}$ as in cut 2 in Fig. 2, MDC linewidths also vary linearly in ω, i.e., $w_{\mathbf{k}} \propto \omega$. Away from the nodal momentum directions, $\mathbf{v}_0(\mathbf{k})$ varies considerably as in cut 4 and higher of Fig. 2. As a result, MDCs' linewidth deviates from the linear-ω dependence. This accounts for the MDC width of cut 5 shown as an example in Fig. 3 and the higher cuts. If the MDC linewidth is multiplied by the bare velocity at each $\mathbf{k}$ in any direction, a linear dependence of the width with ω is obtained both in theory and in the experiments.

(iii) Comparing Figs. 2(d)–2(f), we can see that there are two distinct reasons for the waterfalls. If $\epsilon_{\mathbf{k}}$ reaches $\omega_1 - \mathrm{Re}\Sigma(\omega_1)$ at $\mathbf{k} \approx \mathbf{k}_0$ as $\mathbf{k}$ is varied along the momentum cut, e.g., cut 2 in Fig. 2, $\varepsilon(\mathbf{k})$ follows the waterfall between ω_1 and ω_2, which correspond to E_1 and E_2 defined in experiments.

If the momentum cuts are sufficiently away from the nodal cut such that the bottom of the band is very shallow, $\epsilon_{\mathbf{k}}$ never reaches $\omega_1 - \mathrm{Re}\Sigma(\omega_1)$, e.g., cuts 5–8 in Fig. 2. The observed dispersion $\varepsilon(\mathbf{k})$ then follows Eq. (6) to its maximum value at the bottom of the band $\mathbf{k}_m$. For higher energies, there are no solutions to Eq. (6). In this case the MDC curves stay centered at $\mathbf{k}_m$, which leads to another type of waterfall. E_1 in this case is nearly the energy of the bottom of the renormalized band, and gets continuously smaller as the bottom of the band (where the velocity is zero) becomes continuously more shallow from the (π, π) to the $(\pi, 0)$ direction. The variation of the position of the waterfalls, Fig. 3 of Ref. [8] and Fig. 3 of Ref. [6] is thereby explained. In addition, the linewidth is no longer given by $\mathrm{Im}\Sigma/v_0$, leading to an additional cusp in linewidth at E_1 (e.g., cut 5 in Fig. 3).
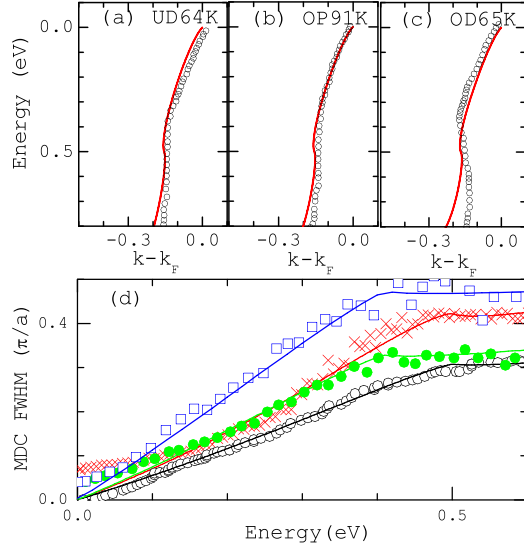
FIG. 4 (color online). Comparison between experimental and theory results (represented by symbols and lines, respectively) for various cuprate samples. (a)–(c) Calculated dispersions for three Pb-doped Bi2212 samples along the nodal cuts: UD with $T_c = 64$ K, OP with $T_c = 91$ K, and OD with $T_c = 65$ K. The experimental data shown are extracted from Fig. 1 of Ref. [3]. The tight-binding fitting parameters of the band structure are taken from Ref. [25]. All these samples are fitted by the parameters $\omega_c = 0.5$ eV (for all) and $\lambda_0 = 0.98$, 1.01, and 1.05, respectively. (d) The MDC linewidths (full width at half-maximum) for different cuprate samples. $\bigcirc$, $\times$, $\bullet$, and $\square$ represent OP-Bi2201 (nodal cut, Ref. [9]), OP-Bi2212 (nodal cut, Ref. [26]), LSCO 0.17 (cut 2 in Fig. 2 of Ref. [8]), and LSCO 0.145 (cut 1 in Fig. 3 of Ref. [27]), respectively. The corresponding theory fitting parameters are $\lambda_0 = 0.99$, $\omega_c = 0.5$ eV; $\lambda_0 = 1.01$, $\omega_c = 0.5$ eV; $\lambda_0 = 1.09$, $\omega_c = 0.41$ eV; and $\lambda_0 = 1.64$, $\omega_c = 0.41$ eV.

However, if radial cuts are taken to avoid the shallow band, the position of the waterfall in momentum space is always the locus of **k** where $\varepsilon(\mathbf{k}) \approx \omega_1$. This locus is shown in Fig. 2(a) for radial cuts and is to be compared with data in Fig. 4 of Ref. [8] and Fig. 4 of Ref. [6].

Concluding remarks.—The experimental results discussed place strong constraints on a theory applicable to the cuprates. Specifically, the experiments give a scattering rate linear in ω up to a sharp cutoff at ω_c and constant above with a coefficient that is a weak function of **k**. This behavior is found in the entire "strange metal" region of the phase diagram. We do not know any ideas proposed for cuprates besides those discussed here that give these properties.

In this Letter, we have pointed out the universal aspects of the measured single-particle self-energy in cuprates and shown that its functional form and even its magnitude is consistent with the recent microscopic theory of quantum-critical fluctuations [11]. These fluctuations are predicated on the existence of an unusual symmetry breaking in

underdoped cuprates for which considerable experimental evidence has also been adduced.

[1] J. C. Campuzano, M. R. Norman, and M. Randeria, in *The Physics of Superconductors*, edited by K. H. Bennemann and J. B. Ketterson (Springer, Berlin, 2004), Vol. II, p. 167.
[2] A. Damascelli, Z. Hussain, and Z.-X. Shen, Rev. Mod. Phys. **75**, 473 (2003).
[3] J. Graf *et al.*, Phys. Rev. Lett. **98**, 067004 (2007).
[4] B. P. Xie *et al.*, Phys. Rev. Lett. **98**, 147001 (2007).
[5] T. Valla *et al.*, Phys. Rev. Lett. **98**, 167003 (2007).
[6] J. Graf, G.-H. Gweon, and A. Lanzara, Physica (Amsterdam) **460C**, 194 (2007).
[7] Z.-H. Pan *et al.*, arXiv:cond-mat/0610442.
[8] J. Chang *et al.*, Phys. Rev. B **75**, 224508 (2007).
[9] W. Meevasana *et al.*, Phys. Rev. B **75**, 174506 (2007).
[10] In D. S. Inosov *et al.*, Phys. Rev. Lett. **99**, 237002 (2007), it is pointed out that the variation of the photoemission matrix elements with momentum can lead to misleading conclusions about the spectral function and produce faux waterfalls. To avoid this, one should take seriously only the spectral function deduced from the experiment that obeys Kramers-Kronig relations.
[11] V. Aji and C. M. Varma, Phys. Rev. Lett. **99**, 067003 (2007).
[12] C. M. Varma *et al.*, Phys. Rev. Lett. **63**, 1996 (1989).
[13] T. Valla *et al.*, Science **285**, 2110 (1999).
[14] E. Abrahams and C. M. Varma, Proc. Natl. Acad. Sci. U.S.A. **97**, 5714 (2000).
[15] A. Kaminski *et al.*, Phys. Rev. B **71**, 014517 (2005).
[16] The band structure $\varepsilon_{\mathbf{k}} = -2t(\cos k_x a + \cos k_y a) - 4t' \cos k_x a \cos k_y a - 2t''(\cos 2k_x a + \cos 2k_y a) - \mu$ was used in Ref. [8] to fit the Fermi surface of LSCO, with $t'/t = -0.144$, $t''/t = 0.072$, and $\mu/t = -0.84$. We use the same values with $t = 0.48$ eV consistent with fits to local-density approximation (LDA) calculations, see, e.g., R. J. Radtke and M. R. Norman, Phys. Rev. B **50**, 9554 (1994).
[17] C. M. Varma, Phys. Rev. Lett. **83**, 3538 (1999).
[18] C. M. Varma, Phys. Rev. B **73**, 155113 (2006).
[19] B. Fauqué *et al.*, Phys. Rev. Lett. **96**, 197001 (2006).
[20] A. Kaminski *et al.*, Nature (London) **416**, 610 (2002).
[21] This is a straightforward extension to $\mathbf{q} \neq 0$ of the $\mathbf{q} = 0$ result of Eq. (44) in Ref. [18].
[22] A. B. Migdal, Zh. Eksp. Teor. Fiz. **34**, 1438 (1958) [Sov. Phys. JETP **7**, 996 (1958)].
[23] A. Kanigel *et al.*, Nature Phys. **2**, 447 (2006).
[24] C. M. Varma and L. Zhu, Phys. Rev. Lett. **98**, 177004 (2007).
[25] A. A. Kordyuk *et al.*, Phys. Rev. B **67**, 064504 (2003).
[26] J. Graf and A. Lanzara (private communication).
[27] J. Chang *et al.*, arXiv:0708.2782.